The Electronic Structures of Silicon, Aluminum, and Magnesium in Tetrahedral Coordination with Oxygen from SCF-Xα MO Calculations

J. A. Tossell

Contribution from the Division of Geochemistry, Department of Chemistry, University of Maryland, College Park, Maryland 20742. *Received November 7, 1974*

Abstract: The electronic structures of the oxyanions SiO_4^{4-}, AlO_4^{5-}, and MgO_4^{6-} are calculated using the SCF-Xα scattered wave cluster MO method. The SiO_4^{4-} calculation yields results in good agreement with available X-ray photoelectron, X-ray emission, and optical data for quartz (SiO_2) and other silicates. A detailed analysis of the X-ray spectra of SiO_2 yields an empirical MO diagram with uncertainties in valence orbital energies of <1 eV. The MO contributing most strongly to the stability of the system is the $5t_2$ σ bonding MO of Si 3p and O 2p character. Involvement of the Si 3d orbitals in the chemical bond is found to be small. Calculated orbital energies for AlO_4^{5-} and MgO_4^{6-} are also in agreement with less complete experimental data for minerals containing these oxyanions. The calculated valence band width decreases from 7.4 eV in SiO_4^{4-} to 2.0 eV in MgO_4^{6-}. The valence band–conduction band separation also decreases from 10.2 to 6.5 eV along the series and the lowest conduction band orbital changes from central atom p-like to central atom s-like in character. These changes result in the systematic variations observable in the metal Kβ X-ray emission spectra and uv absorption spectra of these minerals. One of the valence molecular orbitals (the $5a_1$, Si 3s–O 2p bonding orbital) rises in energy dramatically as the central atom changes from Si to Mg; it is postulated that the observed instability of MgO_4^{6-} is associated with the high energy of this orbital.

Classical mineralogical theory depicts the chemical bond in the Si, Al, and Mg oxides as essentially ionic, although recently several authors have adduced evidence for a substantial covalent component.[1,2] Discussion of the issue has been hindered by our previous inability to apply molecular quantum mechanical methods to such compounds and by the absence of experimental data on their electronic structure. Recent advances in molecular orbital theory and in X-ray spectroscopy have removed these impediments. For example, the electronic structure of SiO_2 has recently been studied by a number of MO methods at different levels of approximation, e.g., extended Hückel,[3-5] approximate SCF-LCAO,[6,7] approximate LCLO,[8] minimum basis set ab initio LCAO,[9] and SCF-Xα scattered wave cluster MO.[10] X-Ray photoelectron spectra (XPS) and uv photoelectron spectra (UPS) have been obtained for SiO_2[11] and the X-ray emission spectra (XES) and X-ray absorption spectra (XAS) of SiO_2 and other oxides have been studied in considerable detail.[12-15] Uv spectra have also been obtained for SiO_2 and other minerals.[16-18] In order to interpret the diverse experimental data and to compare bond type from one oxide to another, we performed SCF-Xα scattered wave MO calculations on the series of anion clusters SiO_4^{4-}, SiO_6^{8-}, AlO_4^{5-}, AlO_6^{9-}, MgO_4^{6-}, MgO_6^{10-}. This paper discusses the tetrahedral oxyanion results only.

The utility of the SCF-Xα methods for the rapid, accurate calculation of the electronic structure of complex molecules has been adequately discussed.[19-21] One of the first studies using the SCF-Xα method was of the oxyanions SO_4^{2-} and ClO_4^-.[22] These results are in good agreement with both large basis set ab initio SCF calculations and with XPS results, as is shown in Table I. The method has also been previously applied to the mineralogically important oxyanions TiO_6^{8-}, FeO_6^{9-},[23] and FeO_4^{6-},[24] and preliminary results have been published for SiO_4^{4-}[10] and CrO_6^{9-}.[25] The parameters employed for the SCF-Xα calculations on SiO_4^{4-}, and AlO_4^{5-} and MgO_4^{6-} are given in Table II.

The Nature of the MO's in SiO_4^{4-}

The valence molecular orbital diagram for SiO_4^{4-} has been presented earlier[10] and is reproduced with additions in Figure 1. The valence region is divided into a set of predominantly O 2s type orbitals ($4a_1$ and $3t_2$), a set of σ bonding orbitals ($5a_1$ and $4t_2$), and a set of predominantly O 2p nonbonding orbitals ($5t_2$, 1e, $1t_1$). The lowest lying empty orbitals are the $6t_2$ and $6a_1$, of mixed Si and O character. The highest energy orbitals found in the calculation are the strongly antibonding 2e, $1t_2$, and $7a_1$.

The distribution of electron density between the various regions of the cluster is given for the filled MO's in Table III. In the SCF-Xα method the space of the molecular cluster is divided into atomic regions (I) consisting of spheres centered on the metal or oxygen nuclei, the interatomic region (II) outside the atomic spheres but within an outer sphere enclosing all the atomic spheres, and the outer sphere region (III). None of the occupied MO's has significant density in region III so this region has been omitted from the table. If we divide the density in region II equally between the five atoms of the cluster, we arrive at an approximate figure for the percent metal character in the MO (ΣM in Table III). The highest energy filled orbital, the $1t_1$, has not been included in the tabulation since it is uniformly 100% oxygen in character. In SiO_4^{4-} each of the four highest energy orbitals listed has substantial Si character, although Si participation is clearly greatest for the s-type $5a_1$ orbital. On the other hand, it is also evident that all the orbitals are predominantly of O 2p character. For the $4t_2$ and $5a_1$ bonding orbitals a substantial fraction of the density lies in the interatomic region, indicating strong involvement in chemical bonding.

The Spectral Properties of Quartz

The electronic structure calculation mentioned above may be verified by analysis of the spectral properties of SiO_2, quartz. In fact, quartz is not the most desirable compound for comparison with the SiO_4^{4-} calculation since it is a tektosilicate in which each of the SiO_4^{4-} oxygens is linked to a second Si atom. However, it does contain the SiO_4^{4-} unit only and it is the only silicate for which comprehensive X-ray and optical spectra are available. The XPS spectrum of SiO_2[11] was assigned in ref 10. That assignment is supported by an identical assignment of the ClO_4^{2-} XPS spectra in ref 26. The XPS spectra of the SiO_4^{4-} and ClO_4^- ox-

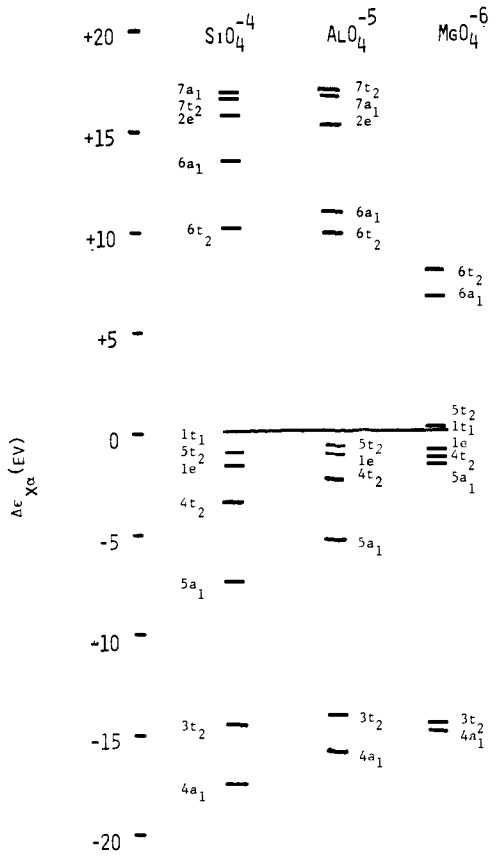

Figure 1. SCF-Xα MO diagrams for SiO_4^{4-}, AlO_4^{5-}, and MgO_4^{6-}.

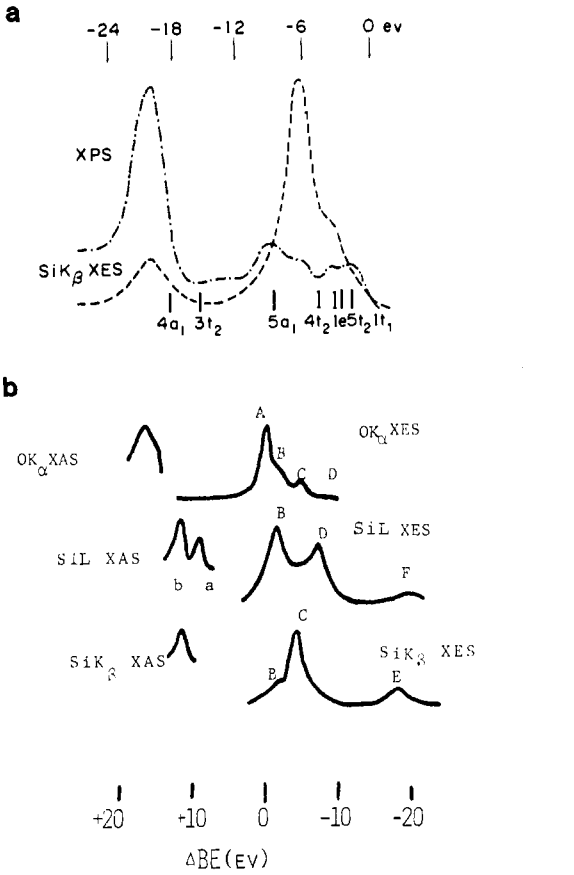

Figure 2. (a) XPS and Si Kβ XES spectra of SiO_2 with SCF-Xα transition state eigenvalues superimposed. (b) XES and XAS spectra of SiO_2.

Table I. Comparison of Experimental and Calculated Relative Orbital Energies for SO_4^{2-} and ClO_4^- (eV)

	SO_4^{2-}			ClO_4^-		
	Exptl[a]	SCF-LCAO[b]	SCF-Xα[c]	Exptl[a]	SCF-LCAO[b]	SCF-Xα[c]
$1t_1$	0	0	0	0	0	0
$5t_2$, 1e	−1.9	−2.5[d]	−1.2[d]	−2.7	−2.5[d]	−1.0[d]
$4t_2$	−5.6	−6.4	−5.4	−7.1	−7.8	−6.8
$5a_1$	−8.5	−9.2	−8.5	−10.2	−11.7	−11.3
$3t_2$	−19.5	−24.1	−16.8	−20.7	−25.4	−17.1
$4a_1$	−23.2	−29.2	−20.8	−28.1	−32.9	−23.4

[a] Reference 26. [b] Reference 27. [c] Reference 22. [d] Weighted average value.

Table II. Parameters Employed in the SCF-Xα Calculations[a]

	R_{M-O}, Å	r_M, Å	r_O, Å	α_M	α_O	$\alpha_{II} = \alpha_{out}$
SiO_4^{4-}	1.609	0.895	0.714	0.727	0.745	0.741
AlO_4^{5-}	1.739	0.940	0.799	0.728	0.745	0.741
MgO_4^{6-}	1.840	0.940	0.900	0.729	0.745	0.741

[a] r_M and r_O are the metal sphere and oxygen sphere radii, respectively; the α's are parameters in the statistical approximation to the exchange potential.

Table III. Distribution of Valence MO Electron Density between Regions of the Cluster in SiO_4^{4-}, AlO_4^{5-}, and MgO_4^{6-} (%)

	I		II	ΣM
	M	O		
		SiO_4^{4-}		
$5t_2$	5.3	65.7	29.0	11.1
1e	1.8	63.6	34.6	8.7
$4t_2$	4.5	57.0	38.5	12.2
$5a_1$	10.8	37.9	51.3	21.1
$3t_2$	5.6	69.6	24.8	10.6
$4a_1$	10.1	59.2	30.7	16.2
		AlO_4^{5-}		
$5t_2$	3.8	67.6	28.6	9.5
1e	1.0	68.0	31.0	7.2
$4t_2$	2.4	61.8	35.8	9.6
$5a_1$	8.5	41.2	50.3	18.6
$3t_2$	2.5	78.4	18.6	6.2
$4a_1$	3.8	72.9	23.2	8.4
		MgO_4^{6-}		
$5t_2$	2.0	75.2	21.4	6.3
1e	0.4	65.7	32.0	6.8
$4t_2$	1.0	59.4	38.0	8.6
$5a_1$	4.1	54.6	41.2	12.3
$3t_2$	0.8	84.2	14.0	3.6
$4a_1$	1.0	81.1	17.2	4.4

yanions are qualitatively similar except that for the chlorate ion a weak feature is observed at high binding energy which is assigned to the $4a_1$ O 2s type orbital. In SiO_2 the intensity of this peak is apparently too low for it to be resolved. The SiO_2XPS spectrum is shown in Figure 2a. It consists of two peaks at low binding energy (A and B), identified with the $1t_1$ and ($5t_2$ + 1e) orbitals, respectively, two peaks at medium binding energy (C and D) assigned to $4t_2$ and $5a_1$ orbitals, and intense peak in the O 2s energy region (E), identified with the $3t_2$ MO. The relative orbital binding energies obtained from the SCF-Xα calculation, using the transition state procedure,[20] are also given in Figure 2a. The $1t_1$ binding energy is chosen to be coincident with that of the lowest binding energy peak in the experimental spectrum. This calibration procedure is necessary since absolute binding energies cannot be obtained accurately from either the SCF-Xα calculation or the XPS experiment. As is evi-

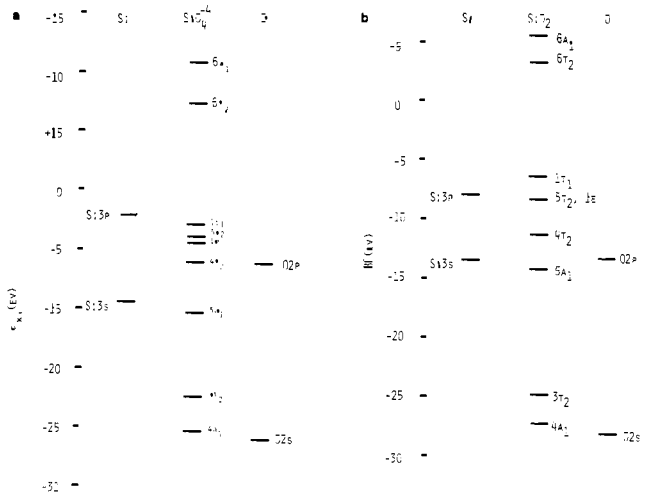

Figure 3 (a) Calculated SiO_4^{4-} correlation diagram. (b) Experimental SiO_2 correlation diagram.

dent in Figure 2a, the calculated relative binding energies are in good agreement with experiment for the bonding and O 2p nonbonding orbital sets but are somewhat too high for the O 2s type orbitals. Figure 2a also shows the Si Kβ XES spectrum of SiO_2, superimposed upon the XPS spectrum by matching the O 2s XPS peak and the low energy Si Kβ satellite peak[12] (usually called Kβ). This alignment is supported by the good agreement of Si Kβ XES and XPS relative energies. For Si Kβ transitions the electric dipole selection rules allow only orbitals of t_2 symmetry to participate. The three features in the Si Kβ spectrum (low energy satellite, main peak, and high energy shoulder) can be assigned immediately to the $3t_2$, $4t_2$, and $5t_2$ MO's. The Si Kβ main peak is found to be coincident in energy with the XPS peak assigned to the $4t_2$ MO while the high energy shoulder is coincident with the $5t_2$ + 1e XPS peak, showing that the relative orbital energies from XPS and Si Kβ XES spectra are indeed remarkably consistent.

The Si L spectrum of SiO_2 obtained by Ershov et al.[14] is shown in Figure 2b. The Si L XES arises from transitions from the valence MO's to a hole in the Si 2p shell and the dipole selection rules allow this transition only for orbitals of a_1 (Si s character) and e and t_2 (Si d character) symmetries. The peak at lowest energy (F in 2b) is therefore assigned to the $4a_1$ orbital and the peak D to the $5a_1$, each of which possesses some Si 3s character. The two highest energy peaks (C and B) are assigned to the $4t_2$ and ($5t_2$ + 1e) orbitals. Using the Si Kα X-ray energy,[28] corresponding to the Si 2p-Si 1s energy difference, for alignment the Si Kβ spectrum is superimposed upon the Si L. As previously stated, the low energy satellite (E) is assigned to the $3t_2$, while the main peak (C) and the high energy shoulder (B) are assigned to the $4t_2$ and $5t_2$ orbitals, respectively. Finally, using the Si 2p and O 1s binding energies from XPS[28,29] we can align the O Kα spectrum of Klein and Chun[15] with respect to the Si L. The symmetry rules are such that all the valence MO's possessing O 2p character could contribute to this spectrum. The main O Kα emission peak (A) lies about 5 eV higher in energy than the main Si Kα peak and fixes the position of the $1t_1$, the highest occupied orbital. Peaks B, C, and D in the O Kα emission spectrum can then be identified with the orbital sets ($5t_2$ + 1e), $4t_2$, and $5a_1$. Since all the orbitals above $3t_2$ possess appreciably O 2p character each will contribute intensity to the O Kα spectrum. Thus the O Kα shows features from all the bonding and O 2p nonbonding MO's in the same way as does the XPS or UPS spectrum although the relative intensities are much different. The energies of peaks A through F in the XPS and the various XES spectra are quite consistent, as shown in Figure 2 and Table IV.

Table IV. Relative MO Energies from Calculation and XPS and XES Data in SiO_2 (eV)

	MO							
	$4a_1$	$3t_2$	$5a_1$	$4t_2$	1e, $5t_2$	$1t_1$	$6t_2$	$6a_1$
SCF-Xα calcd	−17.4	−14.5	−7.4	−3.2	−1.6,−1.0	0	+10.0	+13.5
XPS[a]	−20.8	−18.4	−7.8	−4.8	−1.9	0[g]		
Si K XES,[b] XAS[c]		−18.5		−4.8	−1.9		+10.5	
Si L XES,[d] XAS[e]	−20.4		−7.4	−4.1	−1.9		+9.8	+12.0
O Kα XES[f]			−7.7	−4.7	−1.9	0[g]		

[a] Reference 11. [b] Reference 15. [c] Reference 30. [d] Reference 14. [e] Reference 14. [f] Reference 15. [g] XPS and O Kα XES $1t_1$ levels are set equal.

It is also possible to obtain X-ray absorption spectra of SiO_2, although the experimental difficulties are more formidable. Figure 3b gives the Si L[12] and O Kα absorption spectra for SiO_2 and Si K absorption spectrum for vermiculite.[30] The peaks a, b, and c in the Si L spectrum occur at energies of +9.8, 12.0, and 18.1 eV with respect to the $1t_1$ level. The two lower levels correspond to the $6t_2$ and $6a_1$ empty MO's while the higher peak is associated with the orbitals 2e, $7a_1$, and $7t_2$. The empty orbitals are so high in energy that in our previous work[10] they were found using photoionization transition states. Their orbital energies have been redetermined using a larger Watson charge so as to stabilize all the orbitals. The new energy values are given in Figure 1. Although the $6t_2$ orbital is not changed from previous results the $6a_1$ is now substantially higher in energy. Peak a in the SiL absorption spectrum, at +9.8 eV, may be associated with the $6t_2$ orbital. Peak b in the SiL XAS is assigned to the $6a_1$ orbital. In Figure 3b the Si Kβ XAS spectrum is shown for the mineral vermiculite since ref 13 gives the Si Kβ XAS peak position for SiO_2 but does not show the spectrum. The reported Si Kβ XAS peak position is, however, completely consistent with an assignment to the $6t_2$ orbital, as shown in Table IV. The peak c in the O Kα absorption spectrum of SiO_2, centered at about 16.4 eV, is assigned to the 2e, $7a_1$, and $7t_2$. The assignments of the various XPS and XES spectra along with calculated and experimental values for the energies are summarized in Table IV.

Using the X-ray spectra as a guide the uv spectral features of quartz may also be assigned to individual one-electron transitions. Our earlier assignment[25] assumed that the $6t_2$ and $6a_1$ orbitals were almost degenerate, as found in the previous calculation. Our new results confirm that the separation of peaks a and b in the Si L absorption spectrum probably corresponds to the $6t_2$-$6a_1$ splitting. A definitive assignment of the uv spectrum can be made using the assumption that all the transitions involved take place from the valence band to the lowest energy conduction band orbital, the $6t_2$. The results of this assignment are shown in Table V. The final column gives the orbital energy separations obtained from XES and XAS spectra, and is in good agreement with the optical results. The structure in the uv spectrum therefore arises entirely from the structure of the valence band (although transitions to the $6a_1$ orbital, e.g., $5t_2 \rightarrow 6a_1$ calculated to lie at about 11.8 eV, may also contribute some intensity). Further, there seems to be no distinction between band → band and exciton transitions. The peak at 10.2 eV, often referred to as an exciton peak, does not differ in character from the other peaks.

Table V. Uv Spectral Results for SiO_2

	Exptl uv ΔE^a	XES ΔE^b	Calcd ΔE
$1t_1 \rightarrow 6t_2$	10.2	9.8	10.2
$5t_2, 1e \rightarrow 6t_2$	11.7	11.8	11.1, 11.5
$4t_2 \rightarrow 6t_2$	14.3	14.0	13.3
$5a_1 \rightarrow 6t_2$	17.2	17.3	17.5

[a] Reference 16. [b] References 14 and 15.

Table VI. Calculated and Experimental $K\beta-K\beta'$ Separations in SiO_4^{4-}, AlO_4^{5-}, and MgO_4^{6-} (eV)

	$K\beta-K\beta'$	
	Calcd	Exptl
SiO_4^{4-}	11.3	13.1
AlO_4^{5-}	11.8	14.0
MgO_4^{6-}	13.1	16.2

Orbital Contributions to the Stability of SiO_2

The relationship between MO and component AO energies may be studied in the correlation diagram of Figure 3a. Atomic binding energies are obtained from SCF $X\alpha$ transition state calculations on the free atoms; the MO binding energies are corrected for the difference between the Watson sphere stabilization and the accurate Madelung stabilization.[24] The following facts emerge from an examination of the correlation diagram: (1) the O 2p nonbonding molecular orbitals ($1t_1$, $5t_2$, 1e) are higher in energy than is the O 2p orbital in the free oxygen atom, (2) the $5a_1$-$4t_2$ separation is much smaller than is the 3s-3p separation in the free Si atom, (3) concurrently, the $4t_2$ p-type orbital is strongly stabilized with respect to its Si 3p component, while the $5a_1$ s-type MO shows very little stabilization with respect to the Si 3s.

Nefedov[13] has arrived at very similar conclusions regarding the stabilization of the p-type and s-type bonding orbitals in SiO_2 from X-ray spectral studies. By using experimental ionization energies for the free atoms[31] and calculating absolute MO binding energies by combining O $K\alpha$ XES energies with O 1s and valence band XPS binding energies we can generate an empirical correlation diagram as shown in Figure 3b. Both the calculated and the experimental MO correlation diagrams show the qualitative features just described, although quantitatively the two diagrams differ appreciably. A qualitative analysis of the bonding in SiO_2 should therefore emphasize the stabilization of the $4t_2$ MO during compound formation. The role of the $5a_1$, $5t_2$, and 1e MO's seems to be of lesser importance. This conclusion supports previous workers who have used the main peak Si $K\beta$ XES energy as a measure of the strength of the Si-O bond.[34]

In the SiO_4^{4-} calculation the O 2s orbitals are clearly not strongly involved in bonding; the separation of the $3t_2$ and $4a_1$ orbitals is small and each is higher in energy than is the free atom O 2s. The calculated $3t_2$-$4a_1$ separation is small in agreement with experiment, but each orbital is about 3 eV too high in relative energy. However, the experimental correlation diagram for SiO_2 also shows the $3t_2$ and $4a_1$ to be slightly less stable than the free O 2s. The stability of these O 2s type orbitals does however increase sharply for heavier central atoms from the third period. A striking fact revealed by the valence region XPS[26] of SO_4^{2-} and ClO_4^- is the large splitting of the $3t_2$ and $4a_1$ MO's, which reaches a value of 7.4 eV in ClO_4^-.

Comparison of the $X\alpha$ Results for SiO_4^{4-} with a d-pπ Bonding Model

According to the d-pπ bonding model developed by Cruickshank for third period oxyanions,[32] the 1e MO should contain considerable Si 3d character and should be strongly stabilized with respect to the $5t_2$ orbital, which cannot participate in Si-O d-pπ bonding. Both ab initio and approximate SCF-LCAO calculations which employ Si 3d functions in combination with a minimum basis of s and p orbitals invariably obtain this result. On the other hand, ab initio LCAO calculations employing adequate s,p basis sets find the 1e MO very close in energy to the $5t_2$ and show a much reduced central atom d orbital contribution to the 1e orbital. This result has been demonstrated for SiO[33] and for the series[27] PO_4^{3-}, SO_4^{2-}, ClO_4^-. Johansen (ref 27) also found that the $5t_2$ orbital contained a larger absolute amount of central atom d electron density than did the 1e and that the percentage of central atom d character in the 1e was only 10.2% for SO_4^{2-}. As shown in Table III, a naive partitioning of the innersphere charge obtained in the SCF $X\alpha$ calculation leads to a similar charge distribution in the $5t_2$ and 1e orbitals of SiO_4^{4-}. Both large basis set ab initio calculations and the SCF $X\alpha$ results therefore indicate that the $5t_2$ and 1e orbitals are similar in energy and electron density distribution and contain only about 10% central atom character. Both orbitals are, however, substantially lower in energy than the purely nonbonding $1t_1$ orbital and thus do contribute somewhat to the stability of the material, as is clear from the correlation diagrams. Therefore, Si 3d-O 2p bonding does occur in SiO_4^{4-} but is relatively small in magnitude compared with Si 3s-O 2p and Si 3p-O 2p bonding. Further, it involves σ and π type Si 3d functions in very similar amounts.

Variation within the Series SiO_4^{4-}, AlO_4^{5-}, MgO_4^{6-}

In the binary oxides of Al and Mg the metal atom is six coordinate. Al is commonly found in four coordination in aluminosilicate minerals while four-coordinate Mg is found only in a few unusual minerals, an example being spinel, $MgAl_2O_4$. Experimental data for AlO_4^{5-} and MgO_4^{6-} are consequently more difficult to obtain than was the case for SiO_4^{4-}. However, the available metal $K\beta$ XES and uv spectra do show interesting trends throughout the above series. The separation of the $K\beta'$ peak (assigned to the $3t_2$ MO) and the main $K\beta$ peak (assigned to the $4t_2$ MO) in the M $K\beta$ XES spectrum increases in going from Si to Mg,[12] as shown in Table VI. Our SCF-$X\alpha$ calculations are in qualitative agreement with the experimental results as shown in the table. The variation of the $3t_2$ energy along the series is small, since this orbital is primarily on O 2s nonbonding orbital. The $4t_2$ orbital, on the other hand, shifts dramatically to higher energy, indicative of much weaker covalent bonding, so that the $K\beta-K\beta'$ separation increases. The $5t_2$ orbital generates a high energy shoulder which is well resolved in recent SiO_2 spectra. However, this feature is absent in the Mg $K\beta$ spectrum of $MgAl_2O_4$ and poorly resolved in the Al $K\beta$ spectra of aluminosilicates. We calculate the separation of main peak and shoulder to decrease from 2.2 for SiO_4^{4-} to 1.6 for AlO_4^{5-} and MgO_4^{6-}. The results of Dodd and Glen[12] give $K\beta$ peak-shoulder separations of 5.0 for SiO_2 and 3.5 eV for cordierite, containing Al in four coordination. Therefore, although the peak-shoulder separations are larger than those obtained from recent more accurate work,[15] the trend is in the predicted direction.

Absolute values for $4t_2$ binding energies with respect to the vacuum level may be obtained by combining MK XES data and core level binding energies from XPS. Input data for these calculations and final results are shown in Table VII for tetrahedrally coordinated Si, Al, and Mg. The margin of error is large because the experimental data are com-

Table VII. Absolute $4t_2$ Binding Energies from XES and XPS Data

	SiO_4^{4-}	AlO_4^{5-}	MgO_4^{6-}
BE (M 2p)	103.0[a] (SiO_2)	74.2[a] ($CaAl_2Si_2O_8$)	50.3[a] ($MgAl_2O_4$)
E_{K_α} (M 2p → M 1s)	1740.5[b] (SiO_2)	1486.8[b] (cordierite)	1253.7[b] ($MgAl_2O_4$)
E_{K_β} ($4t_2$ → M 1s)	1831.3[b] (SiO_2)	1550.8[b]	1297.0[b] ($MgAl_2O_4$)
BE ($4t_2$)	12.2	10.2	7.0

[a] Reference 29. [b] Reference 12.

piled from several different sources; however, the trend is clear and is in agreement with calculation.

Uv spectra also show systematic shifts as the central cation is changed. Uv spectral studies of mica minerals[17] containing SiO_4^{4-} and AlO_4^{5-} groups commonly show two sets of peaks around 9.5 and 11.3 eV, while quartz shows only single peaks at 10.2 and 11.7 eV. Peaks observed at 9.8 and 11.6 eV in a natural phlogophite mica may be tentatively assigned to the SiO_4^{4-} unit and those at 9.3 and 11.1 eV to the AlO_4^{5-} unit, in accord with the small calculated decrease in relative $6t_2$ orbital energy in the AlO_4^{5-} cluster. The spectral transition energies in MgO_4^{6-} are somewhat better defined, as a result of the studies of Harlow and Shankland[18] on spinel. The lowest energy uv transition in spinel occurs at 8.1 eV and its intensity increases with Mg content in nonstochiometric spinels, so that this feature may be confidently associated with the MgO_4^{6-} groups. As shown in Figure 1 the conduction band of MgO_4^{6-} differs strikingly from that of the Al and Si oxyanions. The $6a_1$ is the lowest empty orbital and the separation of the $6a_1$ and the $5t_2$ (now at the top of the valence band) is only 6.5 eV. The calculated results are therefore in qualitative agreement with experiment although quantitatively the calculated valence-conduction band separation is too small.

Relative Stabilities of the Oxyanions

Inspection of Figure 1 shows that the orbitals differing most in MgO_4^{6-} with respect to their Al and Si counterparts are the $5a_1$, $4t_2$, and $5t_2$ orbitals. This conclusion is reinforced by the change distribution analysis given in Table III. Only in MgO_4^{6-} does the $5t_2$ orbital lie above the $1t_1$. The increase in relative energy of this orbital in passing from AlO_4^{5-} to MgO_4^{6-} is 1.0 eV; the relative $4t_2$ energy increases by about the same amount. However, the binding energy of the M 3p electron also drops by about 1.0 eV from Al to Mg so that the destabilization of atomic and molecular orbitals is similar. The $5a_1$ relative orbital energy rises by 3.7 eV, while the M 3s binding energy changes by only 2.0 eV. The $5a_1$ orbital energy variation is also accompanied by a sharp drop in percent M character. The previous qualitative bonding analysis for SiO_4^{4-} suggests that the stability of the cluster should parallel the sum of the differences between the energies of the molecular orbitals and the energies of their component atomic orbitals. In this respect the M 3p-O 2p bond strength would not appear to change greatly between AlO_4^{5-} and MgO_4^{6-} while a sharp drop does occur in the strength of M 3s-O 2p bonding, resulting in a sharp destabilization of the $5a_1$ MO. The instability of MgO_4^{6-} can therefore be attributed in the MO scheme to a weakening of the M 3s covalency which raises the energy of the $5a_1$ orbital.

Effect of Si-O Distance Variation in Silicates

The orbital energies shown in Figure 1 are those for a SiO_4^{4-} cluster with a SiO distance of 1.609 Å, the experimental value for α quartz. In less highly polymerized silicates the Si-O distance is invariably larger. The olivines, of simplified composition $(Mg, Fe)_2SiO_4$, are insular silicates with Si-O distances of about 1.63-1.64 Å. In order to isolate the direct effect of Si-O distance variation, as opposed to indirect associations of distance with next nearest neighbor cation identity and position, we carried out a SiO_4^{4-} calculation at $R(Si-O) = 1.634$. The relative energy levels at the two different distances are very similar, the only difference being a rise in the σ-bonding orbital energies for the expanded cluster of approximately 0.1 eV. This is in accord with the Si L XES spectrum of Be_2SiO_4[13] which is almost identical with that of quartz. However, although the Si L spectral energies are the same, the Si 2p binding energy is 0.5 eV smaller in Be_2SiO_4 than in quartz,[31] suggesting valence orbital binding energies smaller by the same amount in the insular silicate. The situation is further complicated by the appreciable changes in Si Kβ main peak energy found by White and Gibbs in a large number of different silicates.[34] Although the experimental situation is thus unclear, it is apparent that any substantial differences in silicate XES spectra must arise from factors correlated with the Si-O distance, rather than from the direct effect of distance variation.

Acknowledgment. The computer time for this project was supported in full through the facilities of the Computer Science Center of the University of Maryland. The author gratefully acknowledges support from NASA contract NGL 21-002-033. The SCF-Xα program was kindly supplied by K. H. Johnson of MIT.

References

(1) W. S. Fyfe, *Am. Mineral.*, **39**, 991 (1954).
(2) G. E. Brown, G. V. Gibbs, and P. H. Ribbe, *Am. Mineral.*, **54**, 1044 (1969).
(3) G. V. Gibbs, M. M. Hamil, L. S. Bartell, and H. You, *Am. Mineral.*, **57**, 1578 (1972).
(4) A. J. Bennett and L. M. Roth, *J. Phys. Chem. Solids*, **32**, 1251 (1971).
(5) V. I. Nefedov, *J. Struct. Chem. (Engl. Transl.)*, **8**, 919 (1967).
(6) J. A. Tossell, *J. Phys. Chem. Solids*, **34**, 307 (1973).
(7) A. Breeze and P. G. Perkins, *J. Chem. Soc., Faraday Trans. 2*, 1237 (1973).
(8) K. L. Yip and W. B. Fowler, *Phys. Rev. B*, to be published.
(9) G. A. D. Collins, D. W. J. Cruickshank, and A. Breeze, *J. Chem. Soc., Faraday Trans. 2*, **68**, 1189 (1972).
(10) J. A. Tossell, D. J. Vaughan, and K. H. Johnson, *Chem. Phys. Lett.*, **20**, 329 (1973).
(11) T. H. DiStefano and D. E. Eastman, *Phys. Rev. Lett.*, **27**, 1560 (1971).
(12) G. G. Dodd and G. L. Glen, *J. Appl. Phys.*, **39**, 5377 (1968).
(13) V. I. Nefedov and V. A. Fomichev, *J. Struct. Chem.*, **9**, 107 (1968); **9**, 217 (1968).
(14) O. A. Ershov, D. A. Goganov, and A. P. Lukirskii, *Sov. Phys.-Solid State (Engl. Transl.)*, **1**, 1903 (1966).
(15) G. Klein and H. U. Chun, *Phys. Status Solidi B*, **49**, 167 (1972).
(16) H. R. Phillip, *J. Phys. Chem. Solids*, **32**, 1935 (1971).
(17) A. T. Davidson and A. F. Vickers, *J. Phys. C*, **5**, 879 (1972).
(18) G. E. Harlow and T. J. Shankland, *Geochim. Cosmochim. Acta*, **38**, 589 (1974).
(19) K. H. Johnson, *Adv. Quantum Chem.*, **7**, 143 (1973).
(20) J. C. Slater, "The Self-Consistent Field for Molecules and Solids", Vol. 4, McGraw-Hill, New York, N.Y., 1974.
(21) R. P. Messmer, L. V. Interrante, and K. H. Johnson, *J. Am. Chem. Soc.*, **96**, 3847 (1974).
(22) K. H. Johnson and F. C. Smith, Jr., *Chem. Phys. Lett.*, **7**, 541 (1970).
(23) J. A. Tossell, D. J. Vaughan, and K. H. Johnson, *Amer. Mineral.*, **59**, 319 (1974).
(24) D. J. Vaughan, J. A. Tossell, and K. H. Johnson, *Geochim. Cosmochim. Acta*, **38**, 993 (1974).
(25) B. M. Loeffler, R. G. Burns, J. A. Tossell, D. J. Vaughan, and K. H. Johnson, *Proc. Lunar Sci. Conf., 5th*, in press.
(26) R. Prins and T. Novakov, *Chem. Phys. Lett.*, **9**, 593 (1971).
(27) H. Johansen, *Theor. Chim. Acta*, **32**, 273 (1974).
(28) J. A. Bearden and A. F. Burr, *Natl. Stand. Ref. Data Ser., Natl. Bur. Stand.*, **No. 14** (1967).
(29) V. I. Nefedov, V. A. Urusov, and M. M. Kakhana, *Geochem. Int.*, **9**, 7 (1971).
(30) D. G. W. Smith and K. Norrish, *Natl. Conf. Electron Probe Anal., Proc., 8th* (1973).
(31) C. E. Moore, *Natl. Stand. Ref. Data Ser., Natl. Bur. Stand.*, **No. 3** (1949).
(32) D. W. J. Cruickshank, *J. Chem. Soc.*, 5486 (1961).
(33) T. L. Gilbert, W. J. Stevens, H. Shrenk, M. Yoshimine, and P. Bagus, *Phys. Rev. B*, **8**, 5977 (1973).
(34) E. W. White and G. V. Gibbs, *Amer. Mineral.*, **52**, 985 (1967).